Time-dependent behavior of photorefractive two- and four-wave mixing

Moshe Horowitz, Daniel Kligler, and Baruch Fischer

Department of Electrical Engineering, Technion–Israel Institute of Technology, Haifa 32000, Israel

Received September 21, 1990; revised manuscript received March 27, 1991

A theoretical and experimental study of the temporal response of photorefractive two- and four-wave mixing processes is given. We examine the buildup and the decay of the output signal and the gratings when the input signal beam is turned on and off. For two-wave mixing we have performed an analysis that includes the depleted-pump regime. The experiment was done with a $BaTiO_3$ crystal. The buildup-and-decay behavior is strongly dependent on the coupling constant and the ratio of the signal and pump intensities. From these measurements we obtain the crystal time constant, which was found to have an intensity dependence with a power of -0.7. The coupling constant is extracted from the data of the whole dynamic process of buildup and erasure and not only from the steady-state point, as is usually done. This is the first analytic study, to the best of our knowledge, for the four-wave mixing decay and buildup. We find that the solution for time-dependent four-wave mixing processes (the phase-conjugate mirror and the double phase-conjugate mirror) with undepleted pumps is identical to that for two-wave mixing with unidirectional optical feedback circuits. This similarity provides a direct way to study the stability properties of the devices. We find, for example, that in the unstable regime of four-wave mixing a self-pulsation of the output corresponds to the frequency detuning of the unidirectional two-wave mixing oscillator.

1. INTRODUCTION

The basic photorefractive mechanism in crystals such as BSO, $BaTiO_3$, and $LiNbO_3$ is thought to be well understood. The band transport[1] and hopping[2] models describe the process in the following terms: Electrons (or holes) from impurity levels are excited by a nonuniform light intensity pattern (such as the fringes of two interfering beams), migrate (by diffusion drift or hopping), and are caught in traps, creating an internal space-charge field. Then the electric field induces changes in the index of refraction (phase gratings), which in turn affect the light beams that have induced the effect. This gives rise to interesting self-action features in two-wave mixing (2WM) and four-wave mixing (4WM) processes, with possibilities of gain, oscillators, and self-pumped phase conjugators.[3]

Since the overall photorefractive dynamics, including the wave mixing part, is described by complicated systems of nonlinear partial differential equations, it is hard to obtain a general solution. Research has focused mainly on steady-state properties. Studies of dynamic phenomena have been largely limited to the response of the photorefractive material only, without taking into account the dynamics of the wave coupling effects. Solymar and Heaton[4] presented the first solution for the temporal behavior of the 2WM output signal when the input signal is abruptly turned on. Cronin-Golomb and co-workers[5,6] extended this treatment to include time-varying signals with arbitrary Fourier frequency components. Other studies in 4WM were undertaken by Papen *et al.* and Zozulya *et al.*[7] and by Bledowski and co-workers,[8] and in 2WM they were performed by Feinberg and Anderson[9] and others.[10,11] More recently, Vachss[12] calculated the grating buildup for the 2WM process and obtained a dependence of the grating buildup on the coupling constant. Most of these studies are limited to the undepleted-pump regime.

In the present paper we present a general theoretical and experimental study of the dynamics and the temporal response of photorefractive 2WM and 4WM (Fig. 1). We derive analytic (to our knowledge, the first one for 4WM) and numerical solutions that provide an understanding of the time dependence of the beam coupling, including the effects of erasing the grating in the material by turning off the signal and leaving the pump. Such an erasing process, which takes place in novelty filters,[6] for example, has not been treated previously to our knowledge. We also include in our study of 2WM the depleted-pump regime. We compare our theoretical results with experiments that we have performed with a $BaTiO_3$ crystal. We also show an analogy between each of two 4WM schemes—the phase-conjugate mirror (PCM) [Fig. 1(b)] and the double phase-conjugate mirror (DPCM) [Fig. 1(c)]—and 2WM in an unidirectional ring cavity. This analogy is used to obtain the dynamics and the stability behavior of the 4WM devices. For example, the self-pulsation frequency in the unstable regime of the 4WM is found to correspond to the frequency detuning of the oscillation in the unidirectional 2WM case.

Section 2 deals with photorefractive 2WM. We first derive an analytic solution for writing and erasure of a grating in the photorefractive material, using the undepleted-pump approximation. This solution is based on Cronin-Golomb's theory,[5] except that we apply boundary conditions in the time domain rather than the frequency domain as he does. We thus obtain a simple analytic solution for the cases in which the input signal is turned on or off. In contrast to the solutions presented in earlier studies, we emphasize the dependence of the dynamic

0740-3224/91/102204-14$05.00

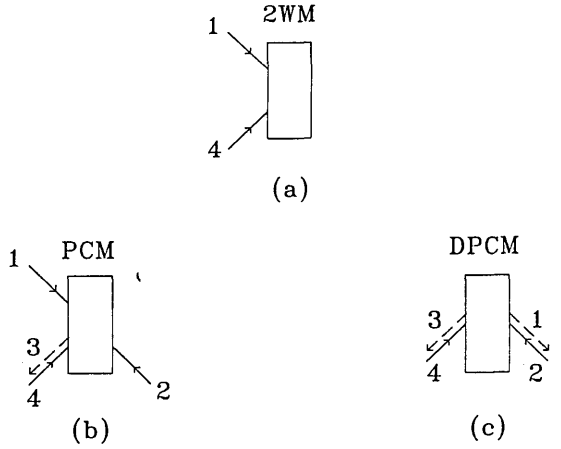

Fig. 1. Schematic of (a) 2WM; (b) 4WM in the standard configuration of a PCM, in which two counterpropagating pump beams, 1 and 2, and an input signal, 4, generate a phase-conjugate beam, 3; and (c) 4WM in the DPCM, in which two nonparallel pump beams, 2 and 4, generate two other beams, 1 and 3.

solution on the coupling of the waves in the photorefractive material.

Next, we present a numerical solution to the 2WM problem for cases in which the signal intensity is not negligible in comparison with that of the pump. In this solution we take into account the nonlinearity of the wave coupling while assuming the material's response to be linear. This numerical solution permits the calculation of the dependence of the writing and erasure times on the ratio of intensities of the signal and pump beams. It also predicts an unusual phenomenon of photorefractive grating buildup after the signal beam has been turned off.

To conclude Section 2, we compare our analytic solution with experimental measurements of 2WM in $BaTiO_3$. This comparison reveals the existence of a photovoltaic field in the material, which affects the dynamics of the wave coupling. It also permits us to estimate the gain coefficient and the time constant of the material simply and precisely.

Section 3 deals with 4WM in a photorefractive cavity. We show an analogy between 4WM and 2WM in a unidirectional ring cavity (in the undepleted-pump approximation). The similarity of the structure demonstrates that there is an effective feedback mechanism in 4WM even when there is no external feedback circuit. This analogy is used to study the 4WM schemes. We present a simple, analytic solution for the time response of writing and erasing a phase-conjugate signal in 4WM.

Finally, we present an analytic solution describing the buildup of oscillation in a DPCM device and calculate the condition for initiation of oscillation.

2. DYNAMIC RESPONSE OF TWO-WAVE MIXING EFFECTS

A. Analytic Solution for Writing and Erasing a Signal in the Undepleted-Pump Approximation

The coupling equations for 2WM in a photorefractive cavity are[1,5]

$$\frac{\partial A_1(z,t)}{\partial z} = -\frac{\gamma}{G} E_{sc}(z,t) A_4(z,t), \tag{1}$$

$$\frac{\partial A_4^*(z,t)}{\partial z} = \frac{\gamma}{G} E_{sc}(z,t) A_1^*(z,t), \tag{2}$$

$$\frac{\partial E_{sc}(z,t)}{\partial t} + \frac{E_{sc}(z,t)}{\tau} = \frac{G}{\tau} \frac{A_1(z,t) A_4^*(z,t)}{I_0}, \tag{3}$$

where γ and G are coupling parameters, τ is the time constant of the material, E_{sc} is the internal electric field in the material, and A_1 and A_4 are the pump and signal fields, respectively. The z direction is perpendicular to the input and output surfaces of the mixing crystal. In the undepleted-pump approximation we obtain

$$\frac{\partial^2 A_4^*(z,t)}{\partial z \partial t} + \frac{1}{\tau} \frac{\partial A_4^*(z,t)}{\partial z} - \frac{\gamma}{\tau} A_4^*(z,t) = 0. \tag{4}$$

Following Ref. 6, we obtain the solution

$$A_4^*(z,t) = \exp(-t/\tau) \sum_{m=0}^{\infty} J_m\left[2\left(-\gamma z \frac{t}{\tau}\right)^{1/2}\right] \times \left[a_m\left(-\gamma z \frac{\tau}{t}\right)^{m/2} + b_m\left(-\frac{t}{\gamma z \tau}\right)^{m/2}\right], \tag{5}$$

where the J_m are the set of Bessel functions and a_m and b_m are constants determined by the boundary conditions. Unlike the approach in Ref. 5, we set the boundary conditions for Eq. (5) in the time domain rather than the frequency domain so as to derive a simple analytic solution. In order to obtain the dynamic response to erasure of the grating, we calculate the strength of the output signal after the input signal is turned off, assuming the system to have been in steady state beforehand [with the known solution $A_4^*(z) = A_4^*(z = 0)\exp(\gamma z) \equiv A_{4,0}^* \exp(\gamma z)$]. Therefore in this case the boundary conditions are

$$A_4^*(z = 0, t) = [1 - U(t)]A_{4,0}^* = \exp(-t/\tau) \sum_{m=0}^{\infty} b_m\left(-\frac{t}{\tau}\right)^m, \tag{6}$$

$$A_4(z, t = 0) = A_{4,0}[\exp(\gamma^* z) - 1] = \sum_{m=0}^{\infty} \frac{a_m^*}{m!} (-\gamma^* z)^m, \tag{7}$$

where $U(t)$ is a step function and $A_{4,0} = A_4(z = 0, t < 0)$. To simplify the right-hand sides of Eqs. (6) and (7), we have used the fact that as $x \to 0$, $J_m(x) \to (x/2)^m/m!$.

Equation (6) can be satisfied for $t > 0$ only if $b_m = 0$ for all m. If we expand $\exp(\gamma^* z)$ as a power series and compare coefficients of z^m in Eq. (7), then we obtain the following expression for the output signal after the input is turned off at $t = 0$:

$$A_4^*(z,t) = A_{4,0}^* \exp(-t/\tau) \sum_{m=1}^{\infty} (-1)^m J_m\left[2\left(-\gamma z \frac{t}{\tau}\right)^{1/2}\right] \times \left(-\gamma z \frac{\tau}{t}\right)^m. \tag{8}$$

In the same manner we can set boundary conditions appropriate to turn on of the signal at the input to a crystal with no preexisting gratings at $t = 0$:

$$A_4(z = 0, t) = A_{4,0} U(t). \tag{9}$$

We then obtain

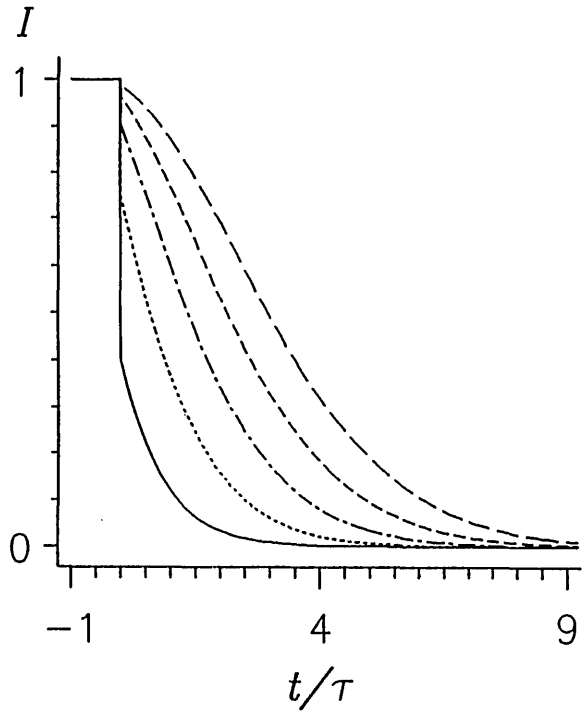

Fig. 2. Theoretical curves for 2WM describing the normalized signal beam intensity versus time after the signal is turned off at $t = 0$ for various positive coupling constants: $\gamma l = 1, 2, 3, 4$, and 5. The lowest curve (fastest decay) corresponds to the lowest γl (=1), and increasing γl decreases the decay rate.

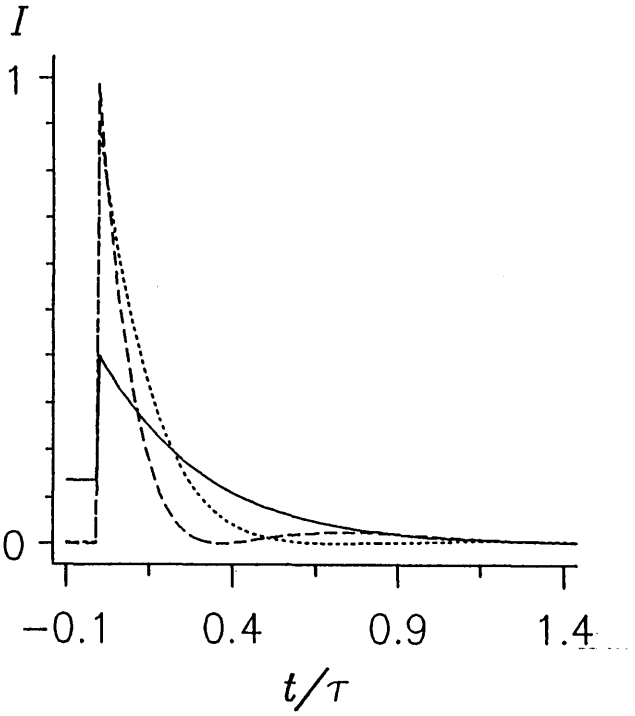

Fig. 3. Theoretical curves for 2WM describing the signal beam intensity versus time after the signal is turned off at $t = 0$ for various negative coupling coefficients: $\gamma l = -1, -3$, and -5. The curve with the fastest decay rate corresponds to the lowest γl (=−5), and increasing γl (up to −1) decreases the decay rate.

$$A_4^*(z,t) = A_{4,0}^* \exp(-t/\tau) \sum_{m=0}^{\infty} (-1)^m J_m\left[2\left(-\gamma z \frac{t}{\tau}\right)^{1/2}\right] \times \left(-\frac{t}{\gamma z \tau}\right)^{m/2}. \quad (10)$$

Figures 2 and 3 show the temporal change of the normalized output intensity from the crystal after the signal is turned off at $t = 0$ as a function of the amplification coefficient γl, where l is the length of the interaction zone. Figure 2 shows the response of a photorefractive amplifier [$\mathrm{Re}(\gamma l) > 0$], while Fig. 3 shows the response of an attenuator [$\mathrm{Re}(\gamma l) < 0$]. In the figures γl was taken to be real (valid for $BaTiO_3$ without applied electric field and frequency detuning).

In Fig. 2 it can be seen that, as the amplification (γl) increases, the normalized response becomes slower and hence the amplification bandwidth decreases. A similar behavior is seen in electronic circuits. This behavior is explained by the fact that at high amplifications, even before the input signal is turned off, the signal energy in the interaction zone in the crystal is drawn mostly from the pump beam, which is scattered by the grating inside the material. Because the grating strength is not altered at the moment the input signal is turned off, the signal inside the crystal remains strong initially, and therefore the output signal drops off slowly.

Figure 3 shows that, when the crystal serves to attenuate the signal [$\mathrm{Re}(\gamma l) < 0$], response times much faster than the time constant of the material (τ) may be obtained. There may also be damped oscillation even in the absence of an external electric field. This phenomenon is explained by the fact that in steady state the signal is attenuated owing to destructive interference between the signal and the portion of the pump beam that is scattered by the grating in the crystal into the signal beam. After the input signal is turned off, the output signal is made up of only the portion of the pump beam that is scattered by the crystal into the signal direction, and therefore the phase of the signal in the interaction zone reverses. The new signal begins to generate a new grating of opposite spatial phase compared with that of the existing grating, leading to rapid erasure of the grating and even to a damped oscillation. These results demonstrate that one can control the response time of a photorefractive device, such as a novelty filter, that is based on 2WM (Ref. 6) by controlling the amplification coefficient through an appropriate choice of the mixing angle.

Figures 4 and 5 show the buildup of the output signal after the input signal is turned on at $t = 0$ for a number of different values of γl, both positive and negative. There is a qualitative similarity to the results in Figs. 2 and 3, particularly in the fact that the larger the value of γl, the slower the change in the output after the input is turned on.

B. Numerical Solution of Two-Wave Mixing with Depletion

For cases in which the signal intensity is nonnegligible and the pump is depleted, the analytic solution in Subsection 2.A is not valid, and we have solved Eqs. (1)–(3) numerically. The assumption in these equations is that the response of the photorefractive material is linear, while the coupling between the two beams in the material is nonlinear. The nonlinearity that does exist in the material gives rise mainly to formation of higher-order gratings.[13] These gratings do not affect the scattering, since they do not fulfill the Bragg condition. Nonlinearity of the material has a negligible effect on the strength of the primary grating, and we therefore neglect it in our calculations.

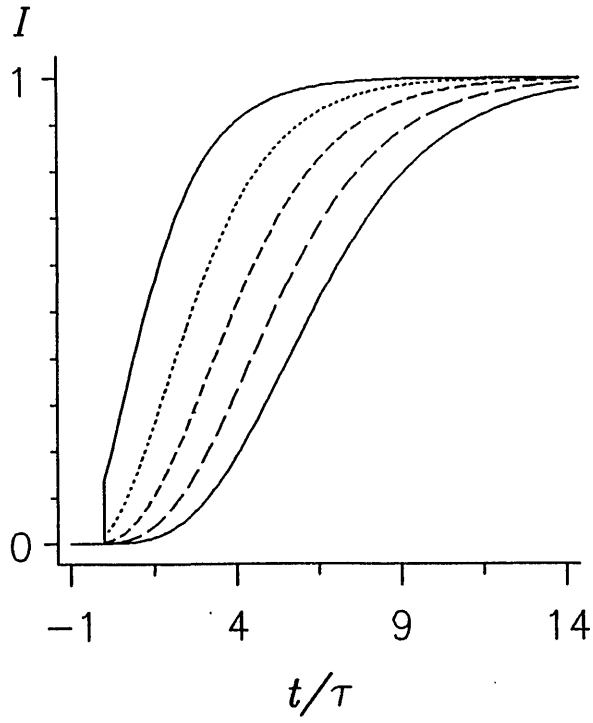

Fig. 4. Theoretical curves for 2WM describing the normalized signal beam intensity versus time after the signal is turned on at $t = 0$ for various positive coupling constants: $\gamma l = 1, 2, 3, 4$, and 5. The highest curve (fastest buildup rate) corresponds to the lowest γl (=1), and increasing γl decreases the buildup rate.

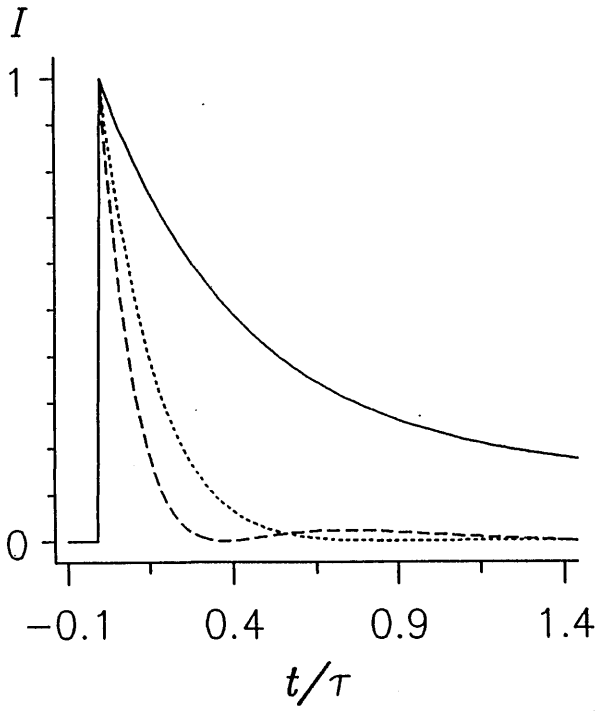

Fig. 5. Theoretical curves for 2WM describing the signal beam intensity versus time after the signal is turned on at $t = 0$ for various negative coupling coefficients: $\gamma l = -1, -3$, and -5. The curve with the fastest buildup rate corresponds to the lowest γl ($=-5$), and increasing γl (up to -1) decreases the buildup rate.

Equations (1)–(3) form a system of partial differential equations dependent on time (t) and position (z). In order to separate these variables, we perform a Taylor expansion in the time domain:

$$A_i(z, t_0 + \Delta t) = \sum_{n=0}^{3} A_{i,n}(z, t_0)(\Delta t)^n, \quad i = 1, 4, \tag{11}$$

$$E_{sc}(z, t_0 + \Delta t) = \sum_{n=0}^{3} E_n(z, t_0)(\Delta t)^n, \tag{12}$$

where $E_0(z, t_0)$, $A_{10}(z, t_0)$, and $A_{40}(z, t_0)$ are given by the initial conditions. In order to find the rest of the coefficients, we substitute Eqs. (11) and (12) into Eqs. (1)–(3) and obtain a set of nine ordinary first-order differential equations dependent on position (z) only. Solving the appropriate set of equations for time t_0 enables us to estimate the electromagnetic fields and the internal field in the material at time $t_0 + \Delta t$. The numerical results give the dependence of the response of the system on the ratio of intensities of the pump and signal beams.

Figures 6 and 7 show the theoretical temporal response of the pump and signal normalized output after the input signal is turned off (Fig. 6) and turned on (Fig. 7). Here τ is the time constant after the signal is turned on or off. As Fig. 6 illustrates, the time needed to erase the grating depends on the modulation depth of the grating recorded in the material, which in turn is a function of the beam ratio. For a weak or strong signal compared with the pump this modulation depth decreases, so that the erasure time is shorter.

In Fig. 6 we also see that for strong signals, after an initial drop at the moment the input signal is turned off, the output signal rises gradually for a significant period before it starts to decay. This increase stems from the fact that at the moment the input signal is turned off, there is a significant drop in the signal strength in the crystal, with a corresponding increase in the pump. This change in turn permits the grating to develop in regions of the crystal where it could not develop previously because the pump was too weak. This new grating increases the scattering efficiency of the pump, with a resultant rise in the strength of the output signal.

Figure 7 shows that the stronger the input signal, the faster the buildup of the output signal. The decrease in buildup time stems in part from the fact that a stronger input signal reduces the grating amplitude required for maximum scattering of the pump beam into the output signal to be attained, since the possible energy transfer from the pump to the signal in this case comes to be limited not by the strength of the grating but by depletion of the pump. Moreover, the buildup rate of the grating increases with increasing modulation depth between the pump and signal beams in the crystal, as indicated by Eq. (3). Thus, during most of the buildup process, the buildup rate of the grating is high, while the grating amplitude required for energy transfer from the pump to the signal is dropping, and therefore the signal buildup time decreases.

These results explain the long buildup time measured in Ref. 14 for fanning relative to that of the output signal. The difference stems from the fact that the strength of the scattered light that gives rise to the fanning is much less than the strength of the input signal to the crystal.

C. Experimental Method and Results

In our experiments we used a poled 7 mm × 6 mm × 3 mm $BaTiO_3$ crystal with the c axis along the 7-mm side, illuminated by an argon-ion laser operating at 515 nm. The optical setup is shown in Fig. 8. The laser beam was

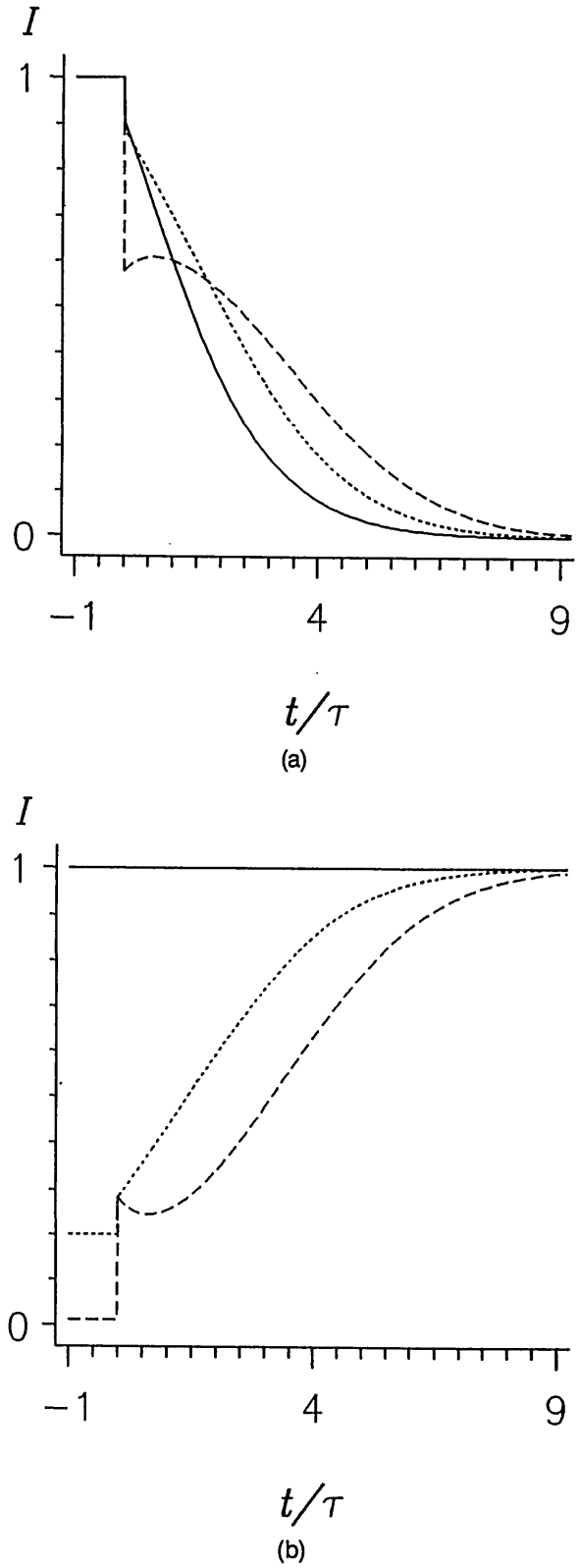

Fig. 6. Theoretical curves for 2WM describing the normalized (a) signal and (b) pump intensities versus time for $\gamma l = 3$ after the signal is turned off at $t = 0$ for various ratios of pump-to-signal intensities: $I_1/I_4 = 10^6$ (solid curves), 100 (dotted curves), and 4 (dashed curves).

split into pump and signal beams, which were focused into the crystal by two lenses with focal lengths of 150 mm. The pump beam diameter was ~1 mm, and the signal beam was 0.4 mm at the crystal face. Both beams had extraordinary polarizations. The difference in the optical path lengths of the pump and signal beams from the laser to the crystal was ~10 cm, considerably less than the laser's coherence length of ~3 m. The pump power enter-

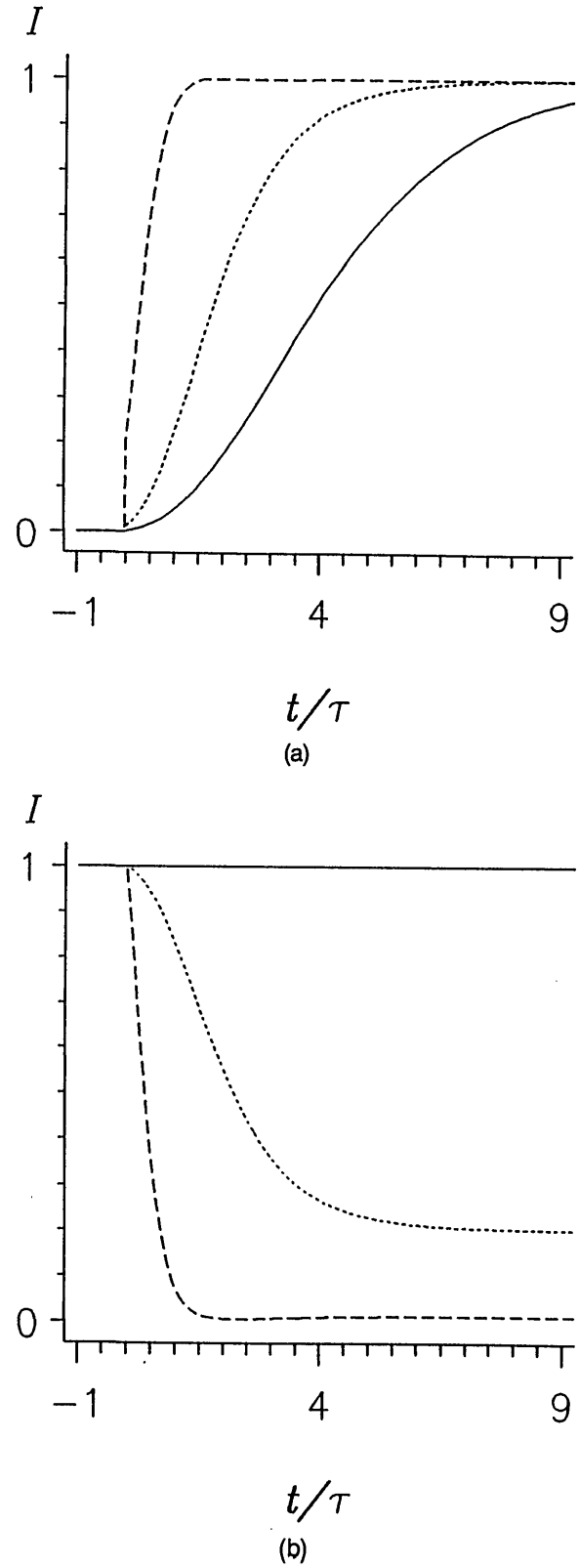

Fig. 7. Theoretical curves for 2WM describing the normalized (a) signal and (b) pump intensities versus time for $\gamma l = 3$ after the signal is turned on at $t = 0$ for various ratios of pump-to-signal intensities: $I_1/I_4 = 10^6$ (solid curves), 100 (dotted curves), and 4 (dashed curves).

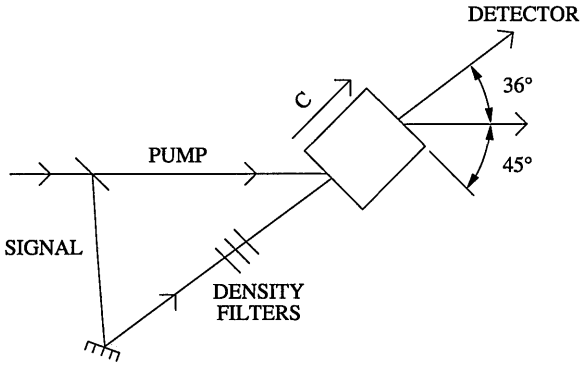

Fig. 8. Experimental arrangement for measuring the dynamics of 2WM in the undepleted-pump approximation. (The specified angles are outside the crystal.)

ing the crystal was varied between 3 and 30 mW. In order to ensure that the system would be linear, we kept the input signal power sufficiently low that decreasing it by 50% from its steady-state value would cause an ~50% decrease in the output signal. This criterion led us to work with weak signals relative to the pump (power ratios of the order of 1:200,000). We therefore saw no changes in the fanning pattern (such as bleaching effects[15]) in the course of our measurements. We controlled the coupling coefficient (γl) by changing the angle between the pump and signal beams (the direction of the signal beam).

In the experiment we measured the temporal response of the output signal after turning the input signal on or off by a simple mechanical shutter. We varied the signal and measured changes in the output only after we first permitted the system to settle for ten minutes or more into a steady state. Since the system's response times were of the order of seconds, we used a pen plotter, connected to the amplified output of a photodetector, to record the changes in the output signal. The plotter graphs were sampled and entered into a computer for analysis. We wrote a computer program to estimate the time constant of the material (τ) and the coupling coefficient (γl) by performing a least-squares fit of our experimental results to the analytic solution given in Subsection 2.A. We emphasize that the fitting was based on common values of τ and γl for the buildup and the erasure processes together for each geometry.

D. Results and Discussion

Figure 9 compares our experimental and theoretical results for buildup of the 2WM output signal after turn on of the input for three values of γl. The figure shows a good fit between the model and the measurements, except at the end of the buildup process, where the experiments show an additional slow buildup (not depicted in Fig. 9). Here the analytic solution gives a well-defined end to the buildup, while the experimental results show a long-lived, additional weak buildup after the primary process is completed. This additional buildup appears to stem from weak scattering from additional gratings generated in regions where the pump intensity is weak and from long-wavelength gratings generated between the signal beam and the fanning. In our analysis we did not take into account the interaction between the fanning of the pump beam and the signal, since this process is slow. The longer the wavelength of the grating in the photorefractive material, the slower its response. Because the wavelengths of the gratings generated between the signal beam and the fanning have much longer components than those of the wavelength of the grating between the signal and the pump, the effect of the signal–fanning interaction is felt only at the end of the output signal variation. To account for the background light due to fanning that entered our measurements, we added a fixed background intensity to our analytic results to obtain a good fit with the experiments.

Figure 10 shows results obtained after the input signal is turned off (erasure of the grating by the pump). We fitted the same coupling constants as those obtained for the buildup process and found good agreement. There is, however, one point that needs more consideration. According to our original model, at the moment the input signal is turned off, the output signal should drop immediately by $\Delta I = [|\exp(\gamma l)|^2 - |\exp(\gamma l) - 1|^2]I_4$, where I_4 is the input signal strength in steady state. If there is no electric field inside the crystal, the coupling coefficient (γl) of the $BaTiO_3$ crystal is real, and there should thus be a significant immediate drop in output signal when the input signal is turned off, as shown in the curves in Fig. 2. For example, for $\gamma l = 3.3$ the signal should drop by 7.25%. This large drop is to be expected despite the weakness of the signal because the scattered pump beam and the signal before it is turned off are in phase, so that constructive interference significantly increases the signal in the crystal.

Our experimental measurements of the immediate output signal drop after the input signal is turned off are much smaller than this theoretical prediction. This discrepancy can be resolved in several ways. One is to suggest that γ is complex, owing to the existence of an electric field in the photorefractive crystal or to detuning

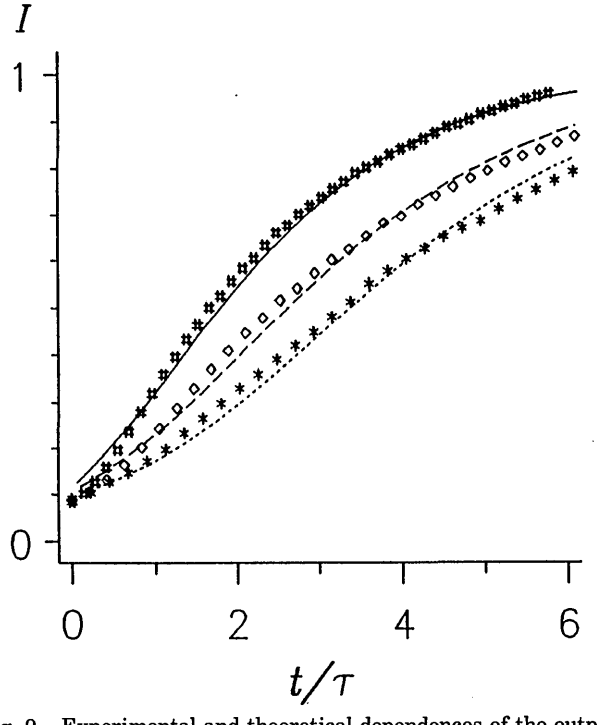

Fig. 9. Experimental and theoretical dependences of the output signal in 2WM after it is turned on. The fitted coupling constants are $\gamma l = 1.72$ (highest curve), 2.78 (middle curve), and 3.3 (lowest curve).

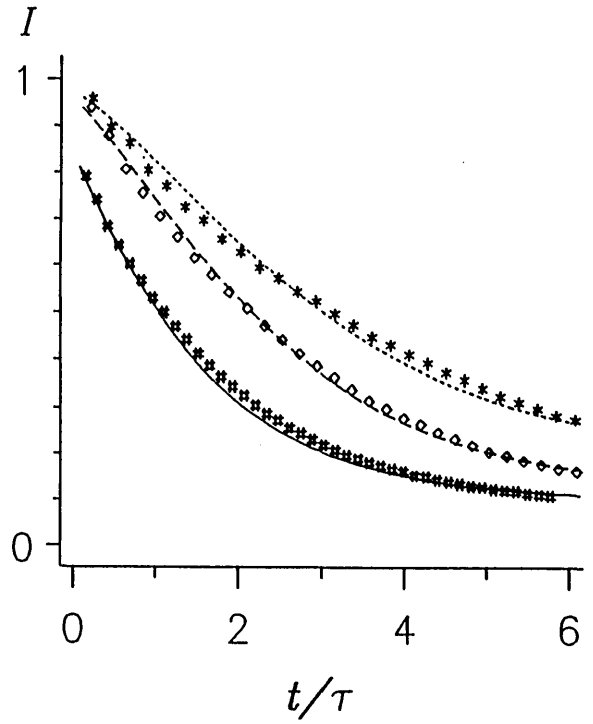

Fig. 10. Experimental and theoretical dependences of the output signal in 2WM after it is turned off. The fitted coupling constants are the same as in Fig. 9.

of $\pm\delta$ of the signal and reflected beams with respect to the pump beams, as given by the equation[3]

$$\gamma = \gamma_0 \frac{E_d + E_p}{E_d} \frac{E_0 + iE_d}{E_0 + i(E_d + E_p)} \frac{1}{1 + i\tau\delta}, \tag{13}$$

where $E_p = ep_d/\epsilon k_g$, $E_d = k_B T k_g/e$, k_B is the Boltzmann constant, T is the temperature, e is the electron charge, ϵ is the dielectric constant, k_g is the wave vector of the grating, and p_d is the trap density. Since our experiment was performed with degenerate frequencies, an internal electric field can explain the signal drop. Assuming that E_d = 2 kV/cm and E_p = 15 kV/cm,[3] we can use Eq. (13) to estimate the strength of the needed field as $E_0 \sim 0.9$ kV/cm. We must note, however, that this is a larger field from the result in Ref. 3, obtained by frequency detuning of a photorefractive oscillator. However, one can also suggest that the relatively small cross sections of the interacting Gaussian beams induce space-charge fields. Other possible explanations can be based on incomplete coherence of the beams or on much larger effective coupling (amplification) constants, such that the amplification part of the output is much larger than our calculated values. There is still a place for a more detailed study of this point.

In addition to reducing the immediate output signal drop when the input signal is turned off, the photovoltaic field also speeds up the increase in output signal when the input signal is turned on and slows down the output signal decay when the input signal is turned off. These considerations improve the fit shown in Figs. 9 and 10 between our theory and experiment.

Finally, Fig. 11 shows the dependence of the estimated time constant of the material (τ) on the pump strength. The plot shows a dependence of time constant on intensity according to

$$\tau = \tau_0 I^{-0.7}.$$

Other researchers have arrived at similar results by different means.[16,17]

3. DYNAMICS OF FOUR-WAVE MIXING CONFIGURATIONS

A. Buildup, Decay, and Stability of the Phase-Conjugate Mirror

Now we discuss the case of 4WM in photorefractive media in the undepleted-pump approximation, in which the pumps are the two external counterpropagating beams {A_1 and A_2 [1 and 2, respectively, in Fig. 1(b)]}. This is the standard phase-conjugate mirror (PCM) scheme. The coupling equations for transmission gratings[18] are

$$\frac{\partial g(z,t)}{\partial t} = \frac{1}{\tau}\left\{-g(z,t) + \frac{\gamma}{I_0}[A_1(z,t)A_4^*(z,t) + A_2^*(z,t)A_3(z,t)]\right\}, \tag{14}$$

$$\frac{\partial A_3(z,t)}{\partial z} = g(z,t)A_2(z,t), \tag{15}$$

$$\frac{\partial A_4^*(z,t)}{\partial z} = g(z,t)A_1^*(z,t), \tag{16}$$

$$\frac{\partial A_1(z,t)}{\partial z} = \frac{\partial A_2(z,t)}{\partial z} = 0, \tag{17}$$

$$g(z,t) = -\frac{i\omega}{2c\cos\theta} r_{\text{eff}} E_{\text{sc}}(z,t), \tag{18}$$

where $E_{\text{sc}}(z,t)$ is the internal field in the material, $A_3(z,t)$ is the phase-conjugate beam of A_4, ω is the optical frequency, c is the speed of light, r_{eff} is the effective linear electro-optic coefficient, 2θ is the angle between beams 1 and 4 (2 and 3), and

$$I_0 = I_1 + I_2, \qquad I_i = |A_i|^2.$$

The boundary conditions are

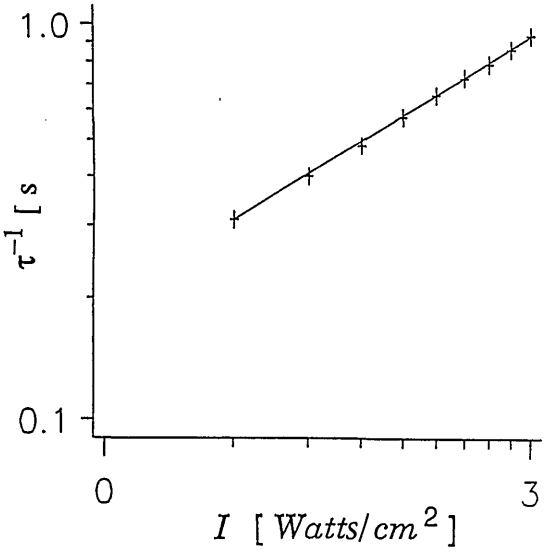

Fig. 11. Experimental dependence on intensity of the estimated time constant. The fit is of $\tau = \tau_0 I^{-0.7}$.

$$A_1(z,t) = A_1, \qquad A_2(z,t) = A_2, \tag{19}$$

$$A_3(z = l,t) = 0, \qquad A_4(z = 0,t) = A_4(0,t), \tag{20}$$

$$E_{sc}(z, t = 0) = E(z,0). \tag{21}$$

In this subsection we derive an analytic solution for the temporal response of the phase-conjugate reflected beam $A_3(z = 0,t)$ leaving the interaction zone after the input signal $A_4(z = 0,t)$ is turned on or off. The coupling equations (15) and (16) give

$$\frac{\partial A_4^*(z,t)}{\partial z} = \frac{A_1^*}{A_2}\frac{\partial A_3(z,t)}{\partial z}. \tag{22}$$

We integrate to obtain

$$A_1^* A_3(z,t) - A_2 A_4^*(z,t) = c(t); \tag{23}$$

$c(t)$ is independent of z. At the boundaries,

$$c(t) = A_1^* A_3(0,t) - A_2 A_4^*(0,t) = -A_2 A_4^*(l,t). \tag{24}$$

Using Eq. (24) in the coupling equations (14)–(18), we obtain

$$\frac{\partial^2 A_3(z,t)}{\partial z \partial t} = \frac{1}{\tau}\left[-\frac{\partial A_3(z,t)}{\partial z} + \gamma A_3(z,t) + \frac{\gamma}{I_0}A_1 A_2 A_4^*(0,t) - \frac{\gamma}{I_0}I_1 A_3(0,t)\right], \tag{25a}$$

$$\frac{\partial^2 A_4^*(z,t)}{\partial z \partial t} = \frac{1}{\tau}\left[-\frac{\partial A_4^*(z,t)}{\partial z} + \gamma A_4^*(z,t) + \frac{\gamma}{I_0}A_1^* A_2^* A_3(0,t) - \frac{\gamma}{I_0}I_2 A_4^*(0,t)\right]. \tag{25b}$$

The two equations for $A_3(z,t)$ and $A_4^*(z,t)$ are separated and similar. We proceed with one of them, the phase-conjugate signal $A_3(z,t)$, in which we are primarily interested. We separate $A_3(z,t)$ into a homogeneous and a particular solution:

$$A_3(z,t) = A_{3H}(z,t) + A_{3P}(t). \tag{26}$$

The homogeneous equation is identical to Eq. (4), which we derived with respect to 2WM in the undepleted-pump approximation, and its solution is therefore given by Eq. (5). The particular solution is

$$A_{3P}(t) = \frac{-A_4^*(0,t)A_1 A_2}{I_0} + \frac{|A_1|^2}{I_0}A_3(z = 0,t). \tag{27}$$

The constants in the homogeneous solution, $\{a_n\}$ and $\{b_n\}$, are given by the boundary conditions.

Before we calculate the constants for our case of turning the input signal on or off, we show here that in the undepleted-pump approximation the problem is identical to the case of 2WM in a unidirectional ring cavity. Using the boundary condition $A_3(z = l,t) = 0$, with the help of Eqs. (26) and (27), we obtain

$$A_3(z = 0,t) = \frac{I_0}{|A_1|^2}\left[\frac{A_4^*(0,t)A_1 A_2}{I_0} - A_{3H}(l,t)\right]. \tag{28}$$

At the other boundary ($z = 0$), again with the use of Eqs. (26) and (27), we obtain

$$A_3(z = 0,t) = \frac{I_0}{|A_2|^2}\left[A_{3H}(0,t) - \frac{A_4^*(0,t)A_1 A_2}{I_0}\right]. \tag{29}$$

Then, combining Eqs. (28) and (29) yields

$$A_{3H}(z = 0,t) = \frac{A_4^*(0,t)A_1 A_2}{|A_1|^2} - A_{3H}(z = l,t)\frac{|A_2|^2}{|A_1|^2}. \tag{30}$$

Because the homogeneous solution for the 4WM case is identical to the 2WM solution in the undepleted-pump approximation, we can use Eqs. (28) and (30) to draw an analogy between 4WM and 2WM in an unidirectional ring cavity as shown in Fig. 12. (A factor of 2 for each 3-dB beam splitter is not included in the scheme.) The internal loop with the crystal corresponds to Eq. (30) and is identical to 2WM with a ring cavity and an additional feedback with a gain (or a loss) coefficient equal to $-I_2/I_1$ for the complex amplitude. In the 2WM ring case the real optical path of the ring cavity determines the phase of the feedback coefficient. The second outer circuit corresponds to Eq. (28). Because 2WM in a ring cavity has been thoroughly researched,[19–22] we can use the similarity to reach a better understanding of 4WM, as we do below in this subsection and in Subsection 3.B.

We begin the solution by calculating the constants of the homogeneous part, $\{a_n\}$ and $\{b_n\}$, for the case in which at $t = 0$ we turn on input signal A_4 into the crystal, which initially contained no gratings:

$$A_4(z = 0,t) = A_{4,0}\,U(t). \tag{31}$$

The constants $\{a_n\}$ are determined by the grating existing in the material at the moment the input A_4 is changed. In our case, with no gratings existing before A_4 is turned on, the phase-conjugate beam $A_3 = 0$ at $t = 0$. Equation (29) then gives

$$A_{3H}(z = 0, t = 0) = \sum_{m=0}^{\infty}\frac{a_m}{m!}(-\gamma z)^m = \frac{A_{4,0}^* A_1 A_2}{I_0}, \tag{32}$$

and therefore

$$a_0 = \frac{A_{4,0}^* A_1 A_2}{I_0},$$

$$a_m = 0 \quad \text{for all } m > 0. \tag{33}$$

To find the constants $\{b_m\}$, we use a power-series expansion of the Bessel functions:

$$J_q(x) = \sum_{m=0}^{\infty}\frac{(-1)^m (x/2)^{2m+q}}{m!(m+q)!}. \tag{34}$$

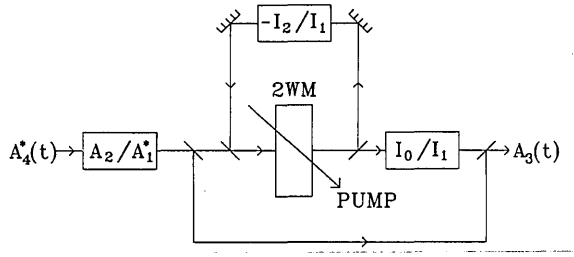

Fig. 12. Circuit for the standard case of the undepleted 4WM (the PCM), which provides the analogy with 2WM in a unidirectional ring resonator. (A factor of 2 for each 3-dB beam splitter is not included in the scheme.)

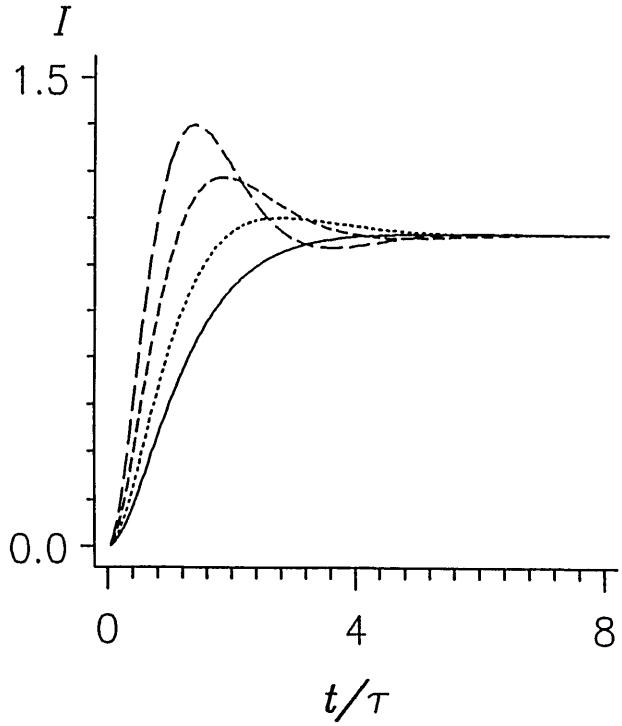

Fig. 13. Normalized intensity of the phase-conjugate beam (I_3 in the 4WM configuration) versus time after the input signal (I_4) is turned on at $t = 0$ for $r = 1$ and various coupling coefficients: $\gamma l = \pm 1, \pm 2, \pm 3$, and ± 4. The curve with the fastest buildup rate corresponds to the highest $|\gamma l|$ (=4), and decreasing $|\gamma l|$ decreases the buildup rate.

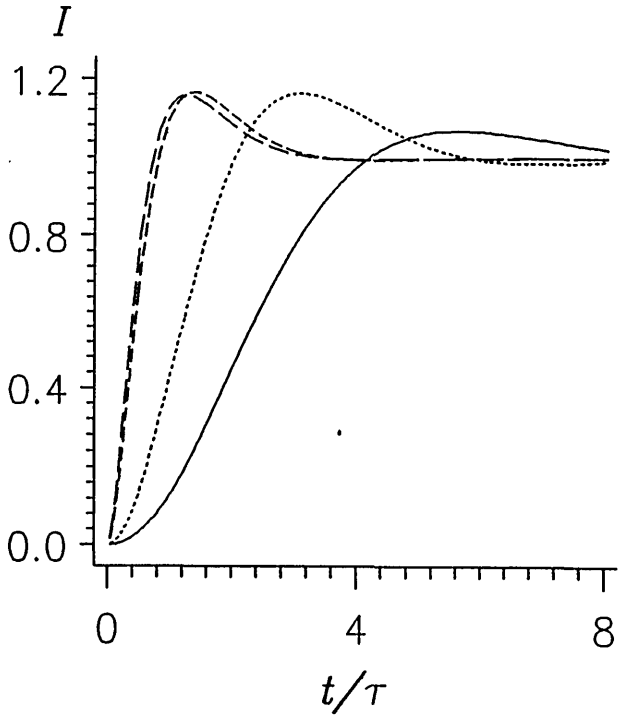

Fig. 14. Normalized intensity of the phase-conjugate beam (I_3) versus time after the input signal (I_4) is turned on at $t = 0$ for $\gamma l = 3$ and various ratios of pump intensities: $r = 1/16, 1/4, 4$, and 16. The curve with the lowest buildup rate corresponds to the lowest r (=0.25), and increasing r increases the buildup rate.

Substituting Eq. (34) into Eq. (30) and comparing coefficients with the same power of t, we obtain a simple system of equations for the $\{b_n\}$:

$$b_0 = -\frac{I_2}{I_1} b_0 + \frac{A_{4,0}{}^* A_1 A_2}{|A_1|^2},$$

$$\left(-\frac{1}{\tau}\right) b_1 = \frac{I_2}{I_1}\left[\frac{(\gamma l)^0}{0!}\frac{b_1}{1!} - \frac{\gamma l}{1!}\frac{b_0}{1!}\right] + \frac{A_{4,0} A_1 A_2}{|A_1|^2}\left(\frac{1}{\tau}\right),$$

$$\vdots$$

$$\left(\frac{1}{n!}\right)\left(-\frac{1}{\tau}\right)^n b_n = (-1)^{n+1}\frac{I_2}{I_1}\left[\frac{(\gamma l)^0}{0!\,n!} b_n - \frac{(\gamma l)^1}{1!\,n!} b_{n-1} + \frac{(\gamma l)^2}{2!\,n!} b_{n-2} + \ldots + \frac{(-1)^n (\gamma l)^n}{n!\,n!} b_0\right] + \frac{A_{4,0}{}^* A_1 A_2}{|A_1|^2}\left(\frac{1}{\tau}\right)^n \frac{1}{n!}. \quad (35)$$

The time dependence of the phase-conjugate reflection is then given by Eq. (28):

$$A_3(z = 0, t) = \frac{I_0}{I_1}\left\{\frac{A_{4,0}{}^* A_1 A_2}{I_0} - \exp(-t/\tau) \sum_{m=0}^{\infty} b_m \times \left(-\frac{t}{\gamma l \tau}\right)^{m/2} J_m\left[2\left(-\gamma l \frac{t}{\tau}\right)^{1/2}\right]\right\}. \quad (36)$$

Figures 13 and 14 show the normalized intensity of the phase-conjugate signal $A_3(0, t)$ during the buildup process as a function of the coupling coefficient γl (real) and the ratio of the intensities of the pump beams, $r \equiv I_2/I_1$. Note that in the above equations the dependence of the pumps can be expressed by r. It can also be shown (according to the argument below of finding the dynamics from the steady-state solution) that the buildup process for given real coupling coefficient γl and pump ratio r is identical to the process for coupling coefficient $-\gamma l$ and pump ratio $1/r$.

We now calculate the temporal response of the phase-conjugate signal at the output of the crystal after the input signal A_4 is turned off at $t = 0$, assuming that the system was previously in steady state, as given by Ref. 18:

$$A_3(z) = \frac{A_2 A_{4,0}{}^*}{A_1{}^*}\left\{\frac{\exp[\gamma(z - l)] - 1}{\exp(-\gamma l) + r}\right\}. \quad (37)$$

To calculate the constants $\{a_n\}$, we must determine the spatial dependence of the phase-conjugate signal after the input is turned off. At that moment the grating will not yet have had time to change, and thus if we follow the previous development, utilizing the analogy between 4WM and 2WM in a ring cavity, we obtain

$$A_{3H}(z, t = 0^+) = \sum_{m=0}^{\infty} \frac{a_m}{m!}(-\gamma z)^m = A_{3H}(z = 0, t = 0^-)[\exp(\gamma z) - 1] + A_{3H}(z = 0, t = 0^+). \quad (38)$$

(The right-hand side is composed of the part of the signal diffracted from the pump before the change plus the new signal, without being affected yet by the crystal.) If we expand $\exp(\gamma z)$ in a power series and compare the coefficients of z^m, we obtain

$$a_0 = A_{3H}(z = 0, t = 0^+),$$

$$a_m = (-1)^m A_{3H}(z = 0, t = 0^-) \quad \text{for } m \geq 1. \quad (39)$$

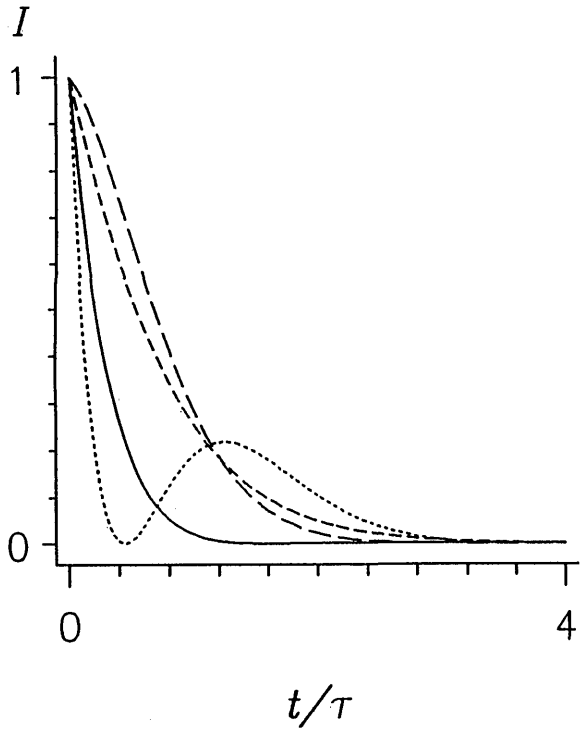

Fig. 15. Normalized phase-conjugate beam versus time after the input signal is turned off at $t = 0$ for various coupling coefficients: $\gamma l = 1$ (solid curve), $\gamma l = 3$ (dotted curve), $\gamma l = -1$ (short-dashed curve), and $\gamma l = -3$ (long-dashed curve).

We find $A_{3H}(z = 0, t = 0^-)$ by comparing the steady-state solution (37) with Eq. (29):

$$A_{3H}(z = 0, t = 0^-) = \frac{A_4^*(z = 0, t = 0^-)A_2}{A_1^*}\frac{I_2}{I_0} \times \frac{\exp(-\gamma l) - 1}{\exp(-\gamma l) + r} + \frac{A_4^*(z = 0, t = 0^-)A_1 A_2}{I_0}. \quad (40)$$

$A_{3H}(z = 0, t = 0^+)$ is given by Eqs. (37) and (28)–(30):

$$A_{3H}(z = 0, t = 0^+) = -(I_2/I_0)A_{3H}(z = 0, t = 0^-) \times [\exp(\gamma l) - 1]. \quad (41)$$

In order to calculate the constants $\{b_n\}$, we insert the constants $\{a_n\}$ that we have already calculated and the power-series expansion of the Bessel functions [Eq. (34)] into Eq. (30) and compare coefficients of powers of t [similar to our method of obtaining Eq. (32)]. Equation (28) then gives the time dependence of the phase-conjugate reflected beam ($t > 0$):

$$A_3(z = 0, t) = -\frac{I_0}{I_1}A_{3H}(l, t) = -\frac{I_0}{I_1}\exp(-t/\tau) \times \sum_{m=0}^{\infty} J_m\left[2\left(-\gamma l\frac{t}{\tau}\right)^{1/2}\right]\left[a_m\left(-\frac{\gamma l\tau}{t}\right)^{m/2} + b_m\left(-\frac{t}{\gamma l\tau}\right)^{m/2}\right]. \quad (42)$$

Figure 15 shows the normalized time dependence of the phase-conjugate signal after turn off of the input signal A_4 for various coupling constants. It shows that, when the input signal is turned off, the nature of the time response of the output depends on the sign of the coupling coefficient γl. This behavior differs from the case of turn on of the input signal, in which the normalized response for given coupling coefficient γl and pump ratio r is identical to that for coupling coefficient $-\gamma l$ and pump ratio $1/r$.

One can obtain the self-oscillation condition and perform a stability analysis of this 4WM system by using the similarity with 2WM in a unidirectional ring oscillator. The condition for starting oscillation for a unidirectional ring is that the overall gain from the crystal and from the feedback loop be unity. Thus, in our 4WM case, with a gain factor in the feedback loop of $-I_2/I_1$ ($=-r$) (as shown in Fig. 12), the condition is

$$\exp(\gamma l)(-r) = 1.$$

Note that the feedback has a negative sign ($-r$) (an out-of-phase feedback), and the condition is identical to that of Ref. 18. For the general instability condition we use the transfer function for photorefractive 2WM,[9] namely, $H(s) = \exp[\gamma l/(s\tau + 1)]$, find the zeros s_0 of $[1 - (-r)H(s)]$, and require that

$$\mathrm{Re}\, s_0 = \mathrm{Re}\left[\frac{\gamma l}{\ln(-1/r)} - 1\right] = \mathrm{Re}\left[\frac{\gamma l}{i\pi n + \ln(1/r)} - 1\right] > 0, \quad (43)$$

where n is an odd integer. A similar condition was obtained from a stability analysis in the Laplace plane in Ref. 7, in the way used in Subsection 3.B for the DPCM. For the case in which γl is real, the steady-state analysis predicts no self-oscillation.[18] Our present analysis, however, shows unstable regions. The minimum coupling coefficient that will give instability is $|\gamma l| = 2\pi$ when $r = \exp(\pm\pi)$.

Figures 16–18 show the temporal behavior in the unstable region after the input signal is turned on or off. It is not surprising to find that at instability the system has a self-pulsation behavior with a frequency that corresponds to the frequency detuning (with respect to the pump frequency) of the unidirectional ring oscillation[20,21] to make up for the out-of-phase feedback. This is described in Figs. 16 and 17 for signal turn off and in Fig. 18 for signal turn on. Exactly at that edge of the instability regime, $\mathrm{Re}\{s_0\} = 0$. If we take $\gamma = 2\pi$, then $r = \exp(-\pi)$, $\mathrm{Im}\, s_0 = \pm 1$, and the oscillation frequency is $\tau\delta = \pm 1$. Figure 16 describes the intensity of the output signal $A_3 \propto \cos(t/\tau)$. This exactly matches the frequency detuning obtained for the steady-state unidirectional 2WM (see Refs. 20 and 21). For parameters that are deeper in the unstable regime, several oscillation frequencies, which provide the out-of-phase compensation in steady state and have an overall gain of at least unity, are permitted.

B. Buildup and Stability of the Double Phase-Conjugate Mirror

In this subsection we present a derivation of an analytic expression for the beginning of the oscillation buildup in a DPCM device.[3,23,24] It is also a 4WM process in which the strong input pumps are the nonparallel propagating beams A_2 and A_4. In the undepleted-pump approximation the pumps are assumed to be constant, and owing to an oscillation process the other two beams, A_1 and A_3, are generated in the oscillation regime. To analyze the dynamics, we take a third weak input beam, A_1. Then the coupling

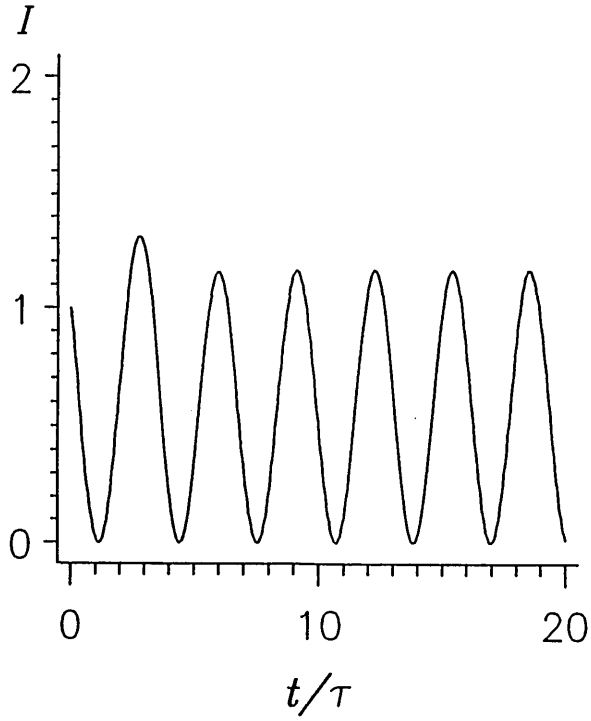

Fig. 16. Normalized phase-conjugate beam versus time after the input signal is turned off at $t = 0$ at the edge of the unstable device [$\gamma l = 2\pi$, $r = \exp(-\pi)$].

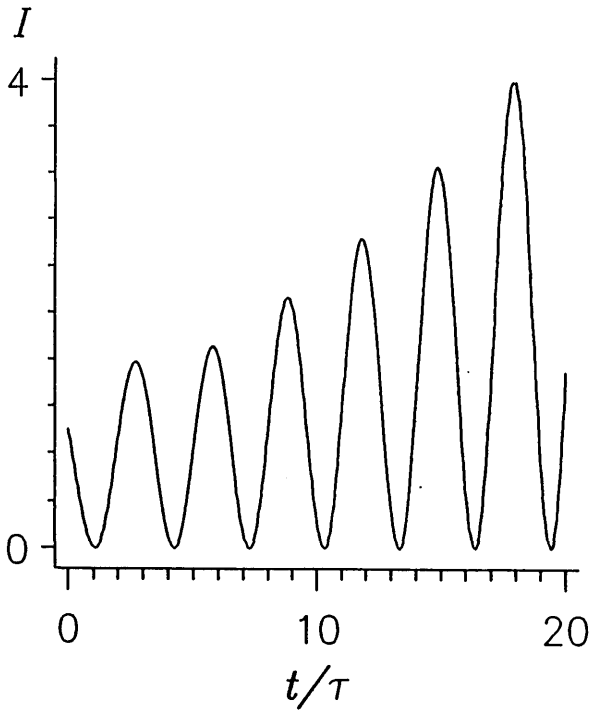

Fig. 17. Normalized phase-conjugate beam versus time after the input signal is turned off at $t = 0$ in an unstable device (slightly above the edge, with $\gamma l = 6.5$ and $r = 0.0432$).

equations are[3,23]

$$\frac{\partial A_1(z,t)}{\partial z} = -g(z,t)A_4(z,t), \tag{44}$$

$$\frac{\partial A_3(z,t)}{\partial z} = g(z,t)A_2(z,t), \tag{45}$$

$$\frac{\partial A_2(z,t)}{\partial z} = \frac{\delta A_4(z,t)}{\delta z} = 0, \tag{46}$$

$$\frac{\partial g(z,t)}{\partial t} = \frac{1}{\tau}\left\{-g(z,t) + \frac{\gamma}{I_0}[A_1(z,t)A_4^*(z,t) + A_2^*(z,t)A_3(z,t)]\right\}, \tag{47}$$

where $g(z,t)$ is defined by Eq. (18) and $I_0 = |A_2|^2 + |A_4|^2$. The boundary conditions are

$$A_1(z = 0,t) = \epsilon(t), \qquad A_2(z,t) = A_2,$$
$$A_3(z = l,t) = 0, \qquad A_4(z,t) = A_4, \tag{48}$$

where $\epsilon(t)$ is the noise-derived scattering in the material, giving rise to the oscillation.

By a derivation similar to the PCM case in Subsection 3.A we obtain

$$A_1(z,t) = \frac{A_4}{A_2}[A_3(z = 0,t) - A_3(z,t)] + \epsilon(t), \tag{49}$$

$$\frac{\partial^2 A_3(z,t)}{\partial z \partial t} = \frac{1}{\tau}\left[-\frac{\partial A_3(z,t)}{\partial z} + p\gamma A_3(z,t) + \frac{\gamma}{I_0}I_4 A_3(z = 0,t) + \frac{\gamma}{I_0}\epsilon(t)A_2A_4^*\right], \tag{50}$$

where $p = (I_2 - I_4)/(I_2 + I_4)$.

The differential equation for the phase-conjugate signal is similar to Eq. (25a). There is an important difference between the two equations, however: The coupling constant in Eq. (25a) is γ, whereas in Eq. (50) the effective coupling constant is $p\gamma$. We separate the solution into

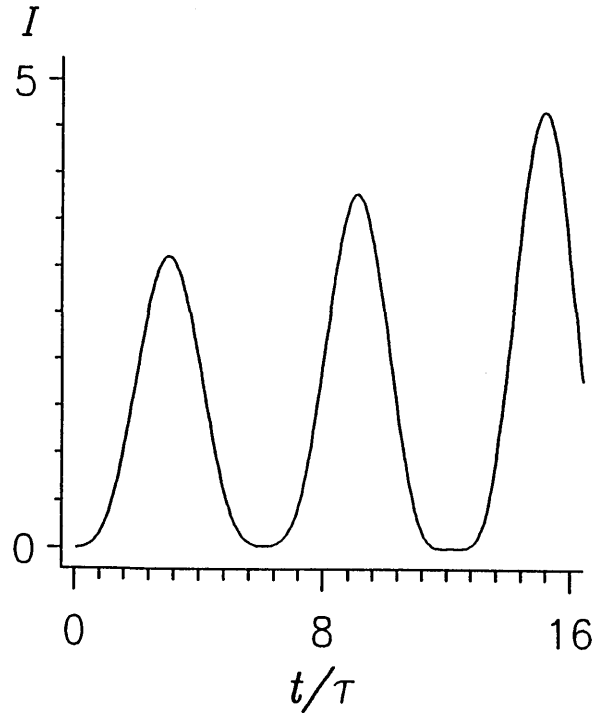

Fig. 18. Normalized phase-conjugate beam versus time after the input signal is turned on at $t = 0$ in an unstable device (slightly above the edge, with $\gamma l = 6.5$ and $r = 0.0432$).

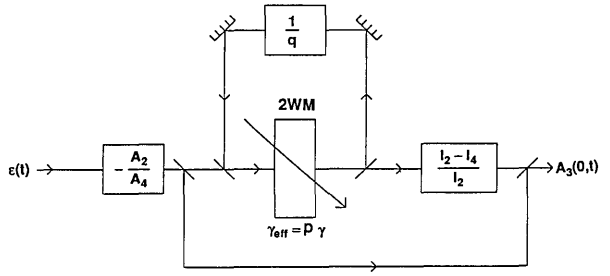

Fig. 19. Circuit for the undepleted DPCM, which provides the analogy with 2WM in a unidirectional ring resonator. (A factor of 2 for each 3-dB beam splitter is not included in the scheme.)

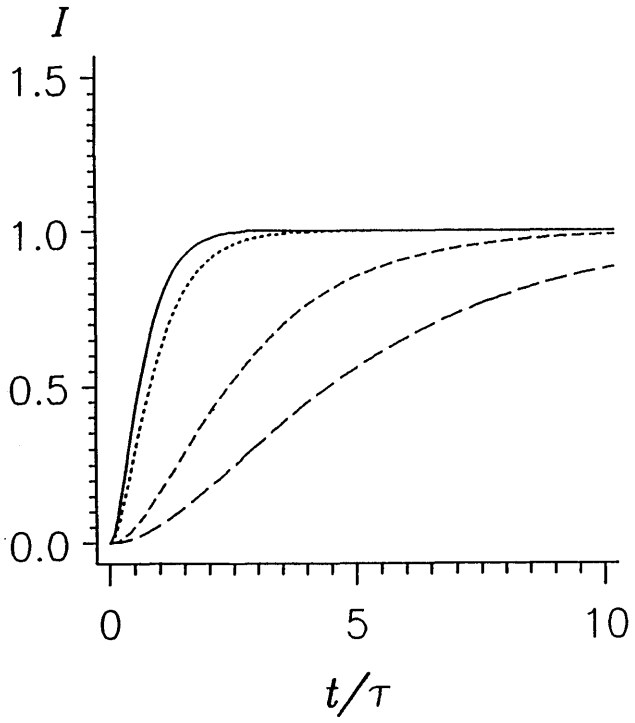

Fig. 20. Normalized phase-conjugate beam (I_1 or I_3) versus time in the DPCM after the input signal is turned on at $t = 0$ for $q = 0.5$ and various coupling constants: $\gamma l = 2$ (solid curve), $\gamma l = 1$ (dotted curve), $\gamma l = -1$ (short-dashed curve), and $\gamma l = -2$ (long-dashed curve).

particular and homogeneous parts:

$$A_3(z,t) = A_{3H}(z,t) + A_{3P}(t). \tag{51}$$

For $I_2 \neq I_4$ the homogeneous equation is identical to the 2WM case in the undepleted-pump approximation [Eq. (4)] with a coupling constant $p\gamma$:

$$A_{3P}(t) = \frac{I_4}{I_4 - I_2} A_3(z = 0,t) + \frac{\epsilon(t)A_2A_4^*}{I_4 - I_2}. \tag{52}$$

Using Eqs. (51) and (52) at the boundary $z = 0$ gives

$$A_{3H}(z = 0,t) = -\frac{I_2A_3(z = 0,t)}{I_4 - I_2} - \frac{\epsilon(t)A_2A_4^*}{I_4 - I_2}, \tag{53}$$

and from the boundary condition $A_3(z = l,t) = 0$ [with Eqs. (51) and (52)] it follows that

$$A_{3H}(z = l,t) = -\frac{\epsilon(t)A_2A_4^*}{I_4 - I_2} - \frac{I_4}{I_4 - I_2} A_3(z = 0,t). \tag{54}$$

Then, from Eqs. (53) and (54) we obtain

$$A_{3H}(z = 0,t) = \frac{I_2}{I_4} A_{3H}(z = l,t) - \frac{\epsilon(t)A_2A_4^*}{I_4}. \tag{55}$$

Again, as in the former 4WM scheme (the PCM), Eqs. (53)–(55) show that in the undepleted-pump approximation the DPCM is similar to the unidirectional ring oscillator based on 2WM. The internal loop in Fig. 19 with the crystal corresponds to Eq. (55) and is identical to 2WM with a ring cavity and an additional (to the crystal gain) feedback with a gain (or loss) coefficient of $q^{-1} \equiv I_2/I_4$. Note, however, the positive feedback sign in the present case (in-phase feedback) compared to the negative (out-of-phase) feedback in the former 4WM configuration. (A factor of 2 for each 3-dB beam splitter is not included in the scheme.) One can obtain the self-oscillation condition and the stability of this 4WM system by using the similarity with 2WM in a unidirectional ring oscillator. The condition for starting oscillation without a mirror,

$$\exp(p\gamma l)q^{-1} = 1,$$

is identical to that of Refs. 3 and 24.

For the general instability condition we again use the transfer function for the photorefractive 2WM,[9] now with an exponential gain of $p\gamma$: $H(s) = \exp[p\gamma l/(s\tau + 1)]$. We find the zeros s_0 of $1 - q^{-1}H(s)$ and require that

$$\mathrm{Re}\, s_0 = \mathrm{Re}\left(\frac{p\gamma l}{\ln q + i2\pi n} - 1\right) > 0, \tag{56}$$

where n is an integer. The instability condition for a real coupling constant (γl) becomes

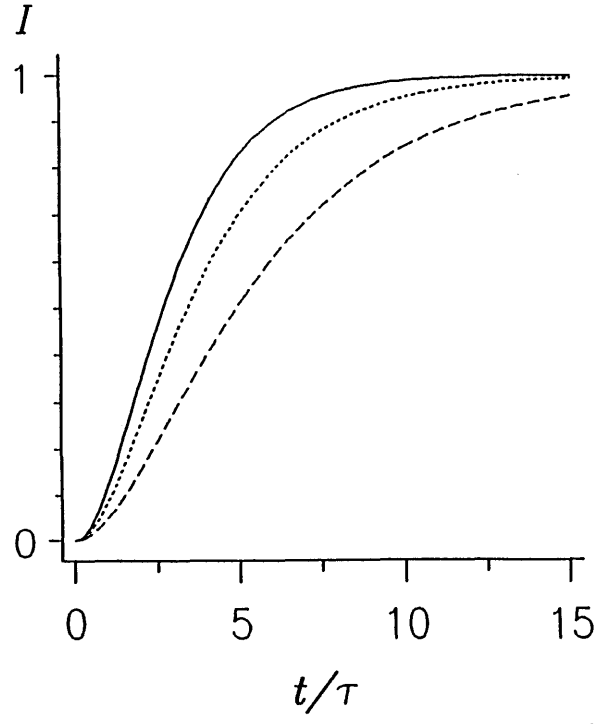

Fig. 21. Normalized phase-conjugate beam (I_1 or I_3) versus time in the DPCM after the input signal is turned on at $t = 0$ for $\gamma l = -1.5$ and various input beam ratios: $q = 0.05$ or 20 (solid curve), $q = 0.2$ or 5 (dotted curve), and $q = 0.95$ or 1.053 (dashed curve).

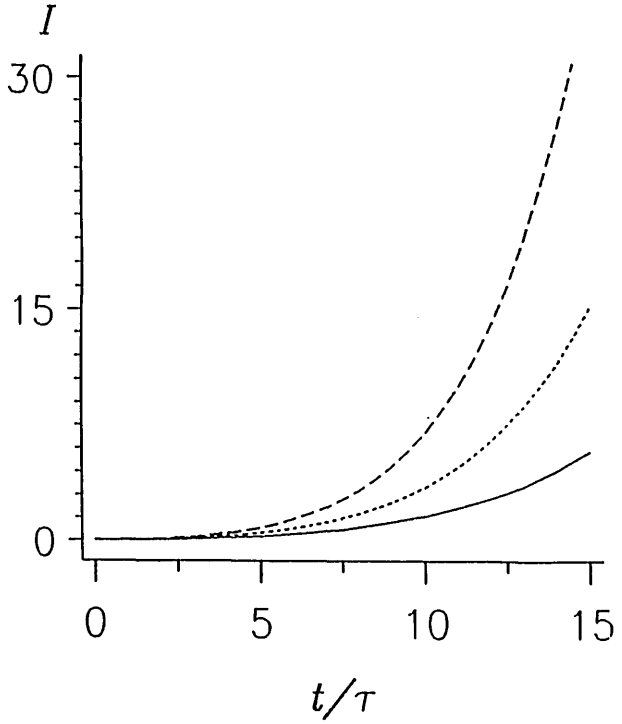

Fig. 22. Normalized intensity of the reflected beam (I_3) versus time after the input signal is turned on at $t = 0$ in the DPCM at an unstable point (close to the threshold) for $q = 0.5$ and $\gamma l = -2.25$ (lowest curve), $\gamma l = -2.3$ (middle curve), and $\gamma l = -2.35$ (highest curve).

$$\gamma l < (\ln q)\frac{1+q}{1-q} < -2, \tag{57a}$$

and that for imaginary γl is

$$\frac{p|\gamma l|2\pi}{(\ln q)^2 + (2\pi)^2} > 1, \tag{57b}$$

with a minimum of $(|\gamma|l)_{\min} \approx 8.7$. We note that the unstable system generates a strong phase-conjugate signal, so that the undepleted-pump approximation is no longer correct. A steady-state solution in the depleted regime is given in Refs. 3 and 23 with an oscillation condition according to Eq. (57a).

Since a detailed analysis of the DPCM by Laplace transform has not been performed yet, we use it here and show that it gives the above stability condition. We define

$$A_3(z,s) = \int_0^\infty A_3(z,t)\exp(-st)\mathrm{d}t. \tag{58}$$

By inserting Eq. (58) into Eq. (50), we obtain

$$\frac{\mathrm{d}A_3(z,s)}{\mathrm{d}z}\left(s + \frac{1}{\tau}\right) = \frac{1}{\tau}\frac{\gamma}{I_0}[A_3(z,s)(I_2 - I_4) + I_4 A_3(z=0,s) + \epsilon(s)A_2A_4^*]. \tag{59}$$

The solution of Eq. (59) is

$$A_3(z,s) = C\exp\left(\frac{p\gamma z}{1+s\tau}\right) + \frac{I_4}{I_4 - I_2}A_3(z=0,s) + \epsilon(s)\frac{A_2A_4^*}{I_4 - I_2}, \tag{60}$$

where the constant C is determined by the boundary condition $A_3(s, z = l) = 0$. Now Eq. (60) gives the transfer function $H(s)$:

$$H(s) = \frac{A_3(z=0,s)}{\epsilon(s)} = -\frac{A_4^*}{A_2^*}\left[\frac{\exp\left(\frac{p\gamma l}{s\tau+1}\right) - 1}{\exp\left(\frac{p\gamma l}{s\tau+1}\right) - q}\right], \tag{61}$$

where $q = I_4/I_2$. In fact, the right-hand side of Eq. (61) is the steady-state ratio between the output and the input with the transformation $\gamma \to \gamma/(s\tau + 1)$. From the general gratings equations[1] it can be shown that such a transformation for the steady-state solution of any photorefractive system will provide the transfer function or the Laplace input–output relation. It immediately gives, for example, the transfer functions for 4WM and 2WM, calculated in Refs. 7 and 9, respectively.

We can obtain from Eq. (61) and the relation $\lim_{t\to\infty} A_3(z=0,t) = \lim_{s\to 0} A_3(z=0,s)$ that for a step input [$\epsilon(s) = \epsilon/s$] the intensity of the phase-conjugate signal in steady state is identical to the intensity calculated in Refs. 3 and 24. From Eq. (61) we have the poles s_0 of the transfer function, and we require that Re $\{s_0\} < 0$ to find the condition for instability. This gives results similar to Eqs. (56) and (57).

When $q = 1$, Eq. (57) collapses to

$$\frac{\partial^2 A_3(z,t)}{\partial z \partial t} = \frac{1}{\tau}\left[-\frac{\partial A_3(z,t)}{\partial z} + \frac{\gamma}{2}A_3(z=0,t) + \frac{\gamma}{2}\epsilon(t)A_2A_4^*\right]. \tag{62}$$

Analysis of Eq. (62) shows that the system is stable for all coupling coefficients and thus will not oscillate.

We solved Eq. (50) to derive the buildup of the phase-conjugate signal in a similar manner to our solution of Eqs. (25) above. Figures 20 and 21 show the buildup process of the phase-conjugate signal in a stable DPCM in the weak-signal approximation as a function of the coupling coefficient Re(γl) and the ratio of the pump intensities, q. Figure 20 shows that, as the amplification approaches the oscillation threshold, the strength of the phase-conjugate signal increases and the normalized buildup rate decreases. The response for the pump ratio q is identical to that obtained for the ratio $1/q$.

Figure 22 shows the buildup process for the phase-conjugate signal in an unstable device as a function of the coupling coefficient.

4. CONCLUSIONS

We have derived solutions for the dynamic behavior of photorefractive two-wave mixing (2WM) and four-wave mixing (4WM) when the input signal to the photorefractive material is turned on or off. We have found analytic solutions for the undepleted-pump (weak-signal) case as well as a numerical solution for 2WM that is valid for strong signals, too. In an experimental study with a $BaTiO_3$ crystal we have measured the transient behavior of the 2WM output signal after turning on or off the (weak) input and found a good fit with our analytic calculations. For the 4WM schemes (phase-conjugate mirror and double

phase-conjugate mirror) we have given an analytic solution in the undepleted-pump approximation and have shown an analogy with 2WM in a unidirectional ring cavity, which provided a picture of the feedback mechanisms and permitted an immediate stability study of the 4WM devices.

Our results provide a better conceptual understanding of the physical processes connected with 2WM and 4WM in photorefractive materials, particularly the dynamic aspects of these processes. In addition, the models that we have presented should be useful in the development of photorefractive devices based on novelty filtering, beam switching and steering, optical computing, and phase conjugation.

ACKNOWLEDGMENTS

This research was performed at the Technion Advanced Opto-Electronics Center, established by the American Technion Society. It was partially supported by a grant from the National Council for Research and Development and the European Economic Community.

REFERENCES

1. N. V. Kukhtarev, V. B. Markov, S. G. Odulov, M. S. Soskin, and V. L. Vinetskii, Ferroelectrics **22,** 949 (1979); **22,** 961 (1979); N. V. Kukhtarev, V. B. Markov, and S. G. Odulov, Opt. Commun. **23,** 338 (1977).
2. J. Feinberg, D. Heiman, A. R. Tanguay, and R. W. Hellwarth, J. Appl. Phys. **51,** 1297 (1980); **52,** 537(E) (1981).
3. B. Fischer, S. Sternklar, and S. Weiss, IEEE J. Quantum Electron. **25,** 550 (1989).
4. L. Solymar and J. Heaton, Opt. Commun. **51,** 76 (1984); L. B. Au and L. Solymar, Appl. Phys. **49,** 339 (1989).
5. M. Cronin-Golomb, in *Digest of Topical Meeting on Photorefractive Materials, Effect and Devices* (Optical Society of America, Washington, D.C., 1987), p. 142.
6. M. Cronin-Golomb, A. M. Biernacki, C. Lin, and H. Kong, Opt. Lett. **12,** 1029 (1987).
7. G. C. Papen, B. A. Saleh, and J. A. Tataronis, J. Opt. Soc. Am. B **5,** 1763 (1988); Opt. Lett. **14,** 287 (1989); A. A. Zozulya and V. T. Tikonchuk, Phys. Lett. A **135,** 447 (1989).
8. A. Bledowski, W. Krolikowski, and A. Kujawski, J. Opt. Soc. Am. B **6,** 1544 (1989); W. Krololikowski, M. Belic, M. Cronin-Golomb, and A. Bledowski, J. Opt. Soc. Am. B **7,** 1204 (1990).
9. J. Feinberg and D. Z. Anderson, IEEE J. Quantum Electron. **25,** 635 (1989).
10. J. Goltz and T. Tshudi, Opt. Commun. **67,** 414 (1988); **68,** 228 (1988); J. Goltz, F. Laeri, and T. Tshudi, Optik (Stuttgart) **71,** 163 (1985).
11. D. R. Erbschloe and T. Wilson, Opt. Commun. **72,** 135 (1989).
12. F. Vachss, in *Digest of Conference on Lasers and Electro-Optics* (Optical Society of America, Washington, D.C., 1990), p. 390; in *Digest of Topical Meeting on Photorefractive Materials, Effect and Devices* (Optical Society of America, Washington, D.C., 1990), p. 140.
13. E. Ochoa, F. Vachss, and L. Hesselnik, J. Opt. Soc. Am. A **3,** 181 (1986).
14. H. Rajbenbach, A. Delboulbe, and J. P. Huingard, Opt. Lett. **14,** 1275 (1989).
15. M. Segev, Y. Ophir, and B. Fischer, Opt. Commun. **77,** 265 (1990).
16. S. Ducharme and J. Feinberg, J. Appl. Phys. **56,** 838 (1984).
17. D. Mahgerefteh and J. Feinberg, Opt. Lett. **13,** 111 (1988).
18. B. Fischer, M. Cronin-Golomb, J. O. White, and A. Yariv, Opt. Lett. **6,** 519 (1981); M. Cronin-Golomb, B. Fischer, J. O. White, and A. Yariv, IEEE J. Quantum Electron. **QE-20,** 12 (1984).
19. J. O. White, M. Cronin-Golomb, B. Fischer, and A. Yariv, Appl. Phys. Lett. **40,** 450 (1982).
20. S. K. Kwong, A. Yariv, M. Cronin-Golomb, and I. Ury, Appl. Phys. Lett. **47,** 460 (1985).
21. P. Yeh, J. Opt. Soc. Am. B **2,** 1924 (1985).
22. G. Pauliat, M. Ingold, and P. Gunter, IEEE J. Quantum Electron. **25,** 201 (1989).
23. S. Weiss, S. Sternklar, and B. Fischer, Opt. Lett. **12,** 114 (1987).
24. B. Fischer, S. Weiss, and S. Sternklar, Appl. Phys. Lett. **50,** 483 (1987).